Journal of Environmental Management 200 (2017) 295–303

Contents lists available at ScienceDirect

Journal of Environmental Management

journal homepage: www.elsevier.com/locate/jenvman

Research article

# The influence of vegetation, mesoclimate and meteorology on urban atmospheric microclimates across a coastal to desert climate gradient

Steven M. Crum*, Sheri A. Shiflett, G. Darrel Jenerette

*Department of Botany and Plant Sciences, University of California, Riverside, CA 92512, USA*

ARTICLE INFO

*Article history:*
Received 31 October 2016
Received in revised form
23 May 2017
Accepted 26 May 2017

*Keywords:*
Air temperature
Relative humidity
Urban heat island
Land use
Urbanization
Ecosystem heterogeneity

ABSTRACT

Many cities are increasing vegetation in part due to the potential for microclimate cooling. However, the magnitude of vegetation cooling and sensitivity to mesoclimate and meteorology are uncertain. To improve understanding of the variation in vegetation's influence on urban microclimates we asked: how do meso- and regional-scale drivers influence the magnitude and timing of vegetation-based moderation on summertime air temperature ($T_a$), relative humidity (RH) and heat index (HI) across dryland cities? To answer this question we deployed a network of 180 temperature sensors in summer 2015 over 30 high- and 30 low-vegetated plots in three cities across a coastal to inland to desert climate gradient in southern California, USA. In a followup study, we deployed a network of temperature and humidity sensors in the inland city. We found negative $T_a$ and HI and positive RH correlations with vegetation intensity. Furthermore, vegetation effects were highest in evening hours, increasing across the climate gradient, with reductions in $T_a$ and increases in RH in low-vegetated plots. Vegetation increased temporal variability of $T_a$, which corresponds with increased nighttime cooling. Increasing mean $T_a$ was associated with higher spatial variation in $T_a$ in coastal cities and lower variation in inland and desert cities, suggesting a climate dependent switch in vegetation sensitivity. These results show that urban vegetation increases spatiotemporal patterns of microclimate with greater cooling in warmer environments and during nighttime hours. Understanding urban microclimate variation will help city planners identify potential risk reductions associated with vegetation and develop effective strategies ameliorating urban microclimate.

Published by Elsevier Ltd.

## 1. Introduction

Metropolitan areas contain a mosaic of land covers that include contrasting patches of high- and low-vegetation intensity and consequently have highly variable ecosystem structures and functions (Grimm et al., 2000). Patterns in vegetation intensity are directly linked to urbanization and mesoclimate distributions (Brazel et al., 2007; Jenerette et al., 2007). Since the mid-20th century, large cities in the United States are warming twice as fast as surrounding rural and wildland areas (Stone et al., 2012), especially in the dry southwestern United States (Brazel et al., 2000). Regional urban warming, commonly described as the urban heat island (UHI), is created by increasing impervious surfaces and decreasing vegetation cover, which warms temperatures in the urban core compared to surrounding rural and wildland areas (Oke, 1973; Santamouris, 2015). However, at finer scales vegetation may create heterogeneous cool refugia within cityscapes (Jenerette et al., 2011; Imhoff et al., 2010; Davis et al., 2016). Vegetation increases latent heat flux via transpiration and decreases sensible heat flux via shading, which cools microclimates (Yang et al., 2011; Jenerette et al., 2011; Chakraborty et al., 2015). Regionally, the magnitude of vegetation cooling is influenced by climate patterns, where, particularly in dryland regions, urbanization may increase vegetation intensity compared to rural and wildland areas. In these regions higher vegetation intensity creates an “oasis effect” and, as a result, reduces summer temperatures within some neighborhoods (Brazel et al., 2000; Jenerette et al., 2007; Buyantuyev and Wu, 2010; Imhoff et al., 2010; Lazzarini et al., 2013; Jenerette et al., 2013). Locally, the distribution of urban vegetation may magnify temperature inequities within a city, resulting in unequal benefits and health consequences for residents (Jenerette et al., 2016). Within cities vegetation cooling is strongest in neighborhoods that are near parks or have high-vegetation cover and water consumption (Shashua-Bar and Hoffman, 2000; Harlan et al., 2009;

* Corresponding author.
*E-mail address:* scrum001@ucr.edu (S.M. Crum).

http://dx.doi.org/10.1016/j.jenvman.2017.05.077
0301-4797/Published by Elsevier Ltd.

Cao et al., 2010; Jenerette et al., 2011; Declet-Barreto et al., 2013). However, increases in relative humidity (RH) associated with highly-vegetated residential ecosystems of arid and semi-arid regions may counter the cooling effect through increases in human-perceived temperatures, as described by the heat index (HI, Steadman, 1979; Hall et al., 2016). HIs are used to combine $T_a$ and RH into a single model that approximates human-perceived equivalent temperature in shaded areas (Rothfusz, 1990). The spatiotemporal distributions of temperature and humidity create an "urban heat riskscape" where microclimates create varying levels of human exposure to heat hazards (Jenerette et al., 2011). Characterizing interactions between vegetation, $T_a$, and RH in urban ecosystems may be useful to predict urban responses to future climate change scenarios.

Patterns and influences of vegetation and landscape factors on fine-scale urban air temperature ($T_a$) within cities have been primarily analyzed using limited weather station data (e.g. Davis et al., 2016), with a small number of studies utilizing a distributed network of sensors (e.g. Feyisa et al., 2014; Hall et al., 2016; Shiflett et al., 2017). These studies have found the greatest $T_a$ differences are typically observed at night and morning hours (Landsberg, 1981; Coseo and Larsen, 2014). Increased nighttime $T_a$ variation likely arises as a consequence of differences in heat flux from urban covers. Impervious surfaces have high heat storage capacity, and thus absorb heat during the day and release it at night, which can create contrasting distributions of air and surface temperatures (Roth et al., 1989; Gallo et al., 1993; Grimmond, 2007; Chakraborty et al., 2015; Hall et al., 2016; Davis et al., 2016). Some studies indicate that urban vegetation at the block or neighborhood scale (<250 m) may influence $T_a$ (Skelhorn et al., 2014; Feyisa et al., 2014), greater than a comparable volume of built cover (Davis et al., 2016). If local vegetation patterns modulate daily changes in $T_a$ through shading effects then the greatest difference between high- and low-vegetated locations should occur at night, because vegetation reduces heat storage and sensible heat flux from urban land covers (Chow et al., 2011). This reduced heat flux is predicted to result in a greater range and temporal variation in $T_a$ for highly vegetated locations. Alternatively, urban vegetation may increase nighttime $T_a$ by providing insulation from high wind velocities (Gillner et al., 2015). Investigations into how urban landscapes affect $T_a$ is essential to uncovering sources of inequities in cooling benefits and developing urban management policies for reducing heat vulnerabilities.

Important drivers that influence the effect of vegetation on $T_a$ may include distributions of mesoclimate and meteorological conditions (Zhao et al., 2014). Mesoclimates, or city-scale climates, with high mean daily temperatures, or heat wave conditions in moderate climates may enhance vegetation cooling and UHI effects by increasing the effect of shading and increasing potential transpiration rates (Jenerette et al., 2011, 2016; Tayyebi and Jenerette, 2016; Ramamurthy and Bou-Zeid, 2017). The negative feedback of vegetation cooling leads to a mean temperature-temperature variability hypothesis (the $\overline{T}_a$–$T_a$ variability hypothesis), that predicts warmer mesoclimates and warmer meteorology will lead to greater $T_a$ spatial variation. Countering mean temperature effects within cities, there is some evidence that precipitation reduces urban heating effects on variation due to increases in air convection and reductions in surface heating (Imhoff et al., 2010; Zhao et al., 2014; Chow et al., 2014). Wind is also predicted to minimize vegetation microenvironment effects through increased air mixing that reduces plant canopy insulating effects and temperature inequities (Grimmond, 2007).

To assess the role of hypothesized drivers of variation in urban $T_a$, we asked: (1) what are the spatiotemporal patterns of summertime vegetation $T_a$ cooling in dryland urban landscapes and (2) if patterns in vegetation intensity are correlated to spatial and temporal variation in $T_a$, how are these variables related to mesoclimate drivers of mean daily temperature, wind, and precipitation? We then expanded this question of microclimate variation by asking: how do vegetation distributions within a dryland city influence the spatiotemporal patterns of summertime RH and HI? To address these questions of variation in vegetation induced microclimate effects, we analyzed the patterns of $T_a$ and RH in response to vegetation, climate, and meteorological sources of variation at three cities along a coastal to inland to desert climate gradient in urban landscapes of the greater Los Angeles metropolitan region of southern California, USA. The combination of a prominent climate gradient of increasing $T_a$ and generally similar patterns of urbanization provide a unique opportunity to study the effects of mesoclimate on urban microclimate. Understanding spatial and temporal variations in $T_a$ and RH across urban landscapes will expand the urban heat "riskscape" concept to include micro-, meso- and regional-scale dynamics of urban microclimates, allowing city planners to better identify the effectiveness of vegetation for urban cooling and reduce heat vulnerabilities, especially in areas of high heat risk.

## 2. Methods

### 2.1. Study sites and design

Our study region is situated in the Los Angeles megacity of 18 million residents within southern California, USA, an area characterized by a Mediterranean climate with hot-dry summers and cool-wet winters. We distributed an $T_a$ sensor network in mature street-side trees in three cities within this region along an approximately 150 km transect from mild coastal Irvine to inland Riverside to hot desert Palm Desert. These cities were selected to test hypotheses of mesoclimate effects on microclimate. Elevation of sensor plots ranged from 4–60 m in Irvine, 238–331 m in Riverside, and 0–144 m in Palm Desert. The surrounding native vegetation community for Irvine and Riverside is Coastal Sage Scrub and Sonoran Desert Scrub for Palm Desert. Across sites, mean annual precipitation (MAP) varies between 300 mm at the coast to 103 mm in the desert. Mean annual temperature (MAT) varies between 17.0 °C at the coast and 23.9 °C in the desert. The climate gradient is more pronounced in summer, when average maximum temperatures in August are 28.4 °C and 41.2 °C in the coastal and desert cities, respectively.

In each of the three cities we established a network of twenty observational pairs, consisting of ten high and ten low vegetation density plots (Fig. 1). Each high- and low-vegetation paired plot was positioned 1–1.5 km apart to quantify local-scale effects of vegetation while accounting for large-scale gradients in $T_a$ related to geography and topography. Sites were selected from high resolution imagery and later confirmed on the ground. We subsequently quantified vegetation differences as differences in the Normalized Difference Vegetation Index (NDVI; Tucker, 1979; Turner et al., 1999), a proxy for vegetation patterns and readily obtained from remotely sensed imagery (van Leeuwen et al., 2006) and commonly used for characterizing urban vegetation (Gallo et al., 1993; Shiflett et al., 2017). We chose NDVI over other indices because of the global availability and high repeat frequency of these data and its association with LST and $T_a$ in prior studies (Jenerette et al., 2016; Shiflett et al., 2017). Average paired-plot level difference in NDVI between all paired high- and low-vegetated plots was 0.22 ± 0.08, 0.31 ± 0.12, and 0.28 ± 0.12 at Coastal, Inland, and Desert cities, respectively (Student's *t*-test $P < 0.05$; Fig. 1E).

Using this design, the average changes in microclimate across paired-plots and correlations of NDVI with microclimate were

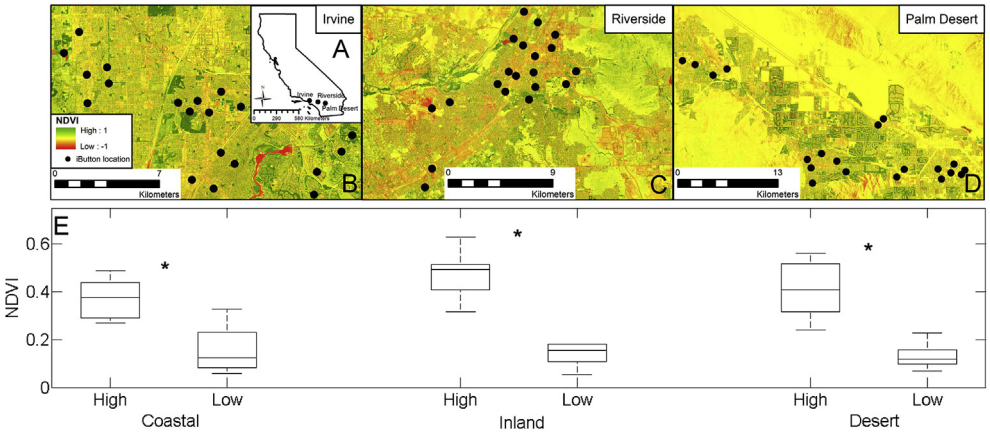


**Fig. 1.** Site locations for summer 2015 and 2016 study periods. **(A)** Coastal to desert transect in southern California including the three study cities Irvine, Riverside, and Palm Desert. **(B,C,D)** NDVI of each city with iButton air temperature sensor locations. Relative humidity and air temperature iButton sensors were placed in the same locations in Riverside during the 2016 study period. All sensors were mounted in street side trees. **(E)** Boxplot of NDVI in high- and low-vegetated locations at 90 m radius resolution along the climate gradient. In all cases high-vegetated sites had greater NDVI than low-vegetated sites using Student's *t*-test ($P < 0.05$).

quantified. All temperature measurements were collected in a 61-day time period in 2015 from July 18th to September 16th (corresponding to Julian day of year (DOY) 199 and 259), encompassing the warmest months of the year. Subsequently, the following summer, relative humidity measurements were collected in the inland city in a 17-day time period from August 17th to September 13th, 2016 (DOY 230 to 257) using the same sampling locations as the $T_a$ measurements.

### 2.2. Micrometeorological sensors

Ten high- and ten low-vegetated plots consisted of three replicate temperature sensors (iButton Thermocron DS1922L, Maxim Integrated Products, Inc., San Jose, California, USA) with an accuracy of ±0.5 °C and range from −10 to 65 °C were mounted on the trunks of three neighboring trees within 10 m of each other 2 m from the ground (n = 180). To explore RH effects, in a follow-up study in 2016 one temperature and humidity sensor (iButton Hydrocron DS1923, Maxim Integrated Products, Inc., San Jose, California, USA) with a temperature accuracy of ±0.5 °C from −10 to 65 °C and RH accuracy of ±0.5% from 0 to 100% was mounted 2 m from the ground on the same trees at each plot in the inland city (n = 20). The added cost of these temperature and humidity sensors limited this design to one replicate per plot in the inland city. The iButton sensors are small, self-contained units with onboard memory, measuring 15 mm in diameter and 5 mm high. Readings were collected hourly throughout the study period. To shield each sensor from direct solar radiation, they were housed in custom polystyrene cylindrical white cups. Additionally, each sensor was mounted on the north side of the trees to avoid any remaining direct effects of solar radiation.

Since the sensors are mounted under tree canopies, $T_a$ and RH may be different than that of open spaces. Prior studies have found that individual tree canopies may increase (Gillner et al., 2015), decrease (Streiling and Matzarakis, 2003; Lin and Lin, 2010), or have no effect on $T_a$ (Armson et al., 2013). Furthermore, both increases and decreases in canopy level RH have been observed (Souch and Souch, 1993; Gillner et al., 2015). While these effects may influence our results, trees were generally pruned, which may minimize their effects at our sensor heights, and our design is a practical solution for embedding sensors within a populated urban environment. To test the accuracy of the custom made radiation shield systems we hung three sensors less than a meter away from a research-grade temperature sensor (HMP-60, Viasala, Helsinki, Finland) housed in a non-aspirated gilled radiation shield underneath an orange tree at the University of California Riverside's Agricultural Operations facility for seven days. Temperature differences between the iButton and the HMP-60 sensors were not observed (2-sample *t*-test, P = 0.64). Furthermore, most iButton measurements fell within two standard deviations of the mean difference (SD = 0.42 °C), with only 2% of measurements below and 2% above this indicator, with no outliers (SD ≥ 3, Osborne and Overbay, 2004).

Reference $T_a$, wind velocity, and precipitation data were obtained from California Irrigation Management Information System (CIMIS) using stations at University of California Irvine's South Coast Research and Extension Center, University of California Riverside's Agricultural Experiment Station, and the Shadow Hills Golf Club in Indio, California (http://cimis.water.ca.gov/WSNReport-Criteria.aspx Accessed Feb/4/2016). These stations were 10.6–26.4, 0.6–11.3, and 4.9–27 km away from iButton plots in Irvine, Riverside, and Palm Desert, respectively. During the study period the average diurnal range in $T_a$ was 10.96 ± 3.52, 13.32 ± 2.95, and 13.64 ± 2.48 °C at Coastal, Inland, and Desert cities, respectively. Furthermore, the average diurnal range during sustained wind periods was 2.40 ± 0.32, 3.71 ± 0.58, and 2.83 ± 0.58 m $s^{-1}$ at Coastal, Inland, and Desert cities, respectively. Although wintertime precipitation was predominant, the summer 2015 study period was unusually wet for coastal and inland regions, following three years of drought. Precipitation from July to September was 65 and 57 mm at the coastal and inland cities, respectively. There were unseasonable rain events at the beginning (DOY 199 to 201) and end (DOY 259) of the study period. For comparison, the average precipitation from July to September is 13 and 10 mm at the coastal and inland cities, respectively. The desert city did not experience above average precipitation with 10 mm of rain, 6 mm below average. Characteristic of summer in this region, no precipitation occurred during the 2016 sampling period.

### 2.3. Remote sensing of vegetation

NDVI was derived from the Airborne Visible/Infrared Imaging Spectrometer (AVIRIS) data from the August 2014 Hyperspectral Infrared Imager (HyspIRI) preparatory mission on a cloud free day. These data were obtained prior to our 2015 and 2016 study periods, but consistency was confirmed visually. In a subsequent study in

Riverside, California, reductions in NDVI between 2014 and 2015 were identified but these changes were proportional to 2014 values (Liang et al., In Revisions). The AVIRIS data collection consists of calibrated images with spectral radiance in 224 10 nm contiguous spectral bands with wavelengths from 400 to 2500 nm (Roberts et al., 2015). Using a scanning mirror, AVIRIS produces 677 pixels for each of the 224 bands on each scan and at the altitude of data collection resulted in a spatial resolution of 20 m pixels. Level 2B post-processed data were used for analysis, which included atmospheric correction using Atmospheric CORection Now (ACORN) software (Roberts et al., 2015). We processed AVIRIS data to obtain NDVI using Eq. (1), where B29 and B51 correspond to AVIRIS spectral channels 29 and 51 with wavelengths 0.64 μm and 0.83 μm.

$$NDVI = B29 - B51/B29 + B51 \quad (1)$$

NDVI was analyzed at each sample plot in post processing using a single pixel and 90 m radius circular buffer.

### 2.4. Analysis

$T_a$, RH, and HI spatial heterogeneity and vegetation effects were quantified with four measures that compared variation in sensor measurements to local land cover distributions. In a preliminary comparison of the individual pixel and 90 m radius buffers, the land cover signal was more pronounced at the 90 m scale, likely in part due to noise at the individual pixel scale, and we chose the 90 m scale for subsequent analyses. Our choice of buffer size agrees with prior research that has found urban microclimate vegetation effects on $T_a$ strongest at scales of 50–500 m (Shashua-Bar and Hoffman, 2000; Feyisa et al., 2014; Davis et al., 2016; Shiflett et al., 2017). First, as a direct measure of vegetation intensity on microclimate, the slope of the linear regression between NDVI and $T_a$ was calculated hourly within each city. Additionally, the slope of the linear regression between NDVI, and RH and HI was calculated hourly within the inland city for 2016. HI was calculated using the Rothfusz (1990) model (EQ 2), which has been adopted by the United States National Weather Service (Steadman, 1979).

$$HI = -42.379 + 2.049(T_a) + 10.143(RH) - 0.225(T_a)(RH) - 0.007(T_a)(T_a) - 0.055(RH)(RH) + 0.001(T_a)(T_a)(RH) + 0.0008(T_a)(RH)(RH) - 0.000002(T_a)(T_a)(RH)(RH) \quad (2)$$

HI is a subjective index of human-perceived temperatures and contains assumptions about human physiology, clothing, solar radiation exposure, and wind velocity (Rothfusz, 1990). Second, the difference between low- and high-vegetated paired plots, expressed as $\Delta T_a$ and ΔRH, was used to evaluate vegetation effects on $T_a$ and RH, respectively. These measures capture the mean $T_a$ and RH difference between paired plots, while accounting for regional sources of climate variation. To obtain plot-level $T_a$ an average was calculated using all three replicates from the 2015 study. Third, the mean $T_a$ and RH difference between high- and low-vegetated plots was expressed as the mean percent change in $T_a$ and RH, calculated by dividing $\Delta T_a$ and ΔRH by mean $T_a$ and RH and expressed as a whole number percent, to show a normalized average. Fourth, the coefficient of variation (CV) was used to quantify spatial and temporal variations. The CV is a dimensionless quantity of variation normalized by the sample mean; commonly expressed as a whole number percent frequently used to assess spatiotemporal landscape variation (Crum et al., 2016). Temporal heterogeneity in vegetation effects on $T_a$ was analyzed at both daily and seasonal scales using correlation between NDVI and temporal CV of $T_a$. Daily-scale spatial averages were analyzed using the slope of correlation in NDVI and $T_a$, percent change in $T_a$, and the slope of correlation in mean $T_a$ and spatial CV of $T_a$. Daily scale temporal variation is the average hourly data using all days of the study period. Seasonal variation includes data from all days of the study period, from DOY 199 to 259.

## 3. Results

### 3.1. Daily patterns in cooling intensity

Vegetation cooling effects, measured as the slope of NDVI and $T_a$, had a consistent daily pattern throughout the climate gradient (Fig. 2). Slopes were generally negative; increases in NDVI tended to decrease $T_a$, although during mid-day hours slopes approached zero or were not significant ($P > 0.05$). Furthermore, slopes decreased along the climate gradient, with hourly average slopes ranging from −0.25 to −3.83 and −1.82 to −6.79, at the coastal and desert cities, respectively. Despite steeper relationships in the desert at night, there were fewer significant correlations compared to coastal and inland cities ($P < 0.05$). Daily changes in the strength of the relationship, measured using the Pearson correlation coefficient, mirrored that of the slope, with the exception of the desert city where we observed weaker nighttime correlations than the other cities (Supplemental Fig. 1). Correlations decreased in the daytime more at the coast than the desert, with r-values decreasing 0.67 at the coast and 0.33 at the desert.

In our follow-up study, vegetation effects on RH, measured as the slope of NDVI and RH, had a strong daily pattern in the inland city (Fig. 3). Slopes were all positive with mean values ranging from 7.41 to 23.93, indicating that increases in NDVI consistently increased RH, with much lower slopes during the mid-day hours. During the evening the effects were driven by large differences in only some pairs. Two paired plots had unusually high nighttime ΔRH, with two hourly values greater than two standard deviations of the mean hourly difference (Supplemental Fig. 2). Unlike correlations found between temperature and NDVI, there was a less noticeable daily pattern in percentage of insignificant correlations for RH ($P > 0.05$). Similar to 2015, slope of NDVI and $T_a$ had a strong daily pattern in the inland city (Fig. 3). This cooling effect was slightly reduced during the day where there were no significant correlations between 12:00 and 18:00 when factoring in heat index values (Fig. 3).

The strength of vegetation effects varied throughout the study period, but generally vegetation cooling effects were greater at night for $\Delta T_a$, the average of the local scale temperature change from low- to high-vegetated plots (Fig. 4). $\Delta T_a$ was mostly positive with values as high as 4.07 °C. There were some exceptions with a reversal in temperature differences, mostly in the daytime hours, with values as low as −0.14 °C. When comparing $\Delta T_a$ during the rainiest day (DOY 259) with the hottest (DOY 252 at the coast and DOY 227 at the inland and desert cities) there were $\Delta T_a$ reductions ($P < 0.001$) of 43% in coastal, 71% in inland, and 32% in desert cities. Along with reduced vegetation effects, the coastal city had 20% reductions in spatial variation between local pairs, while there was increased variation between inland (132%) and desert (32%) cities. Daily averages of local scale vegetation cooling effects from the entire study period were measured as the average $\Delta T_a$ divided by mean $T_a$ or percent change in $T_a$ (Fig. 5). A strong “U-shaped” daily pattern emerged throughout the climate gradient ranging from 1.12% to 8.11%. Furthermore, daily range in vegetation $T_a$ effects increased along the climate gradient, with average percent change in $T_a$ ranging from 1.12 to 4.82% and 1.43–8.11%, at the coastal and desert cities, respectively. Supporting findings from 2015, $\Delta T_a$ for the 2016 campaign for the inland city was the same (Supplemental Fig. 3, $P > 0.05$, Student's *t*-test). There was no daily pattern in ΔRH

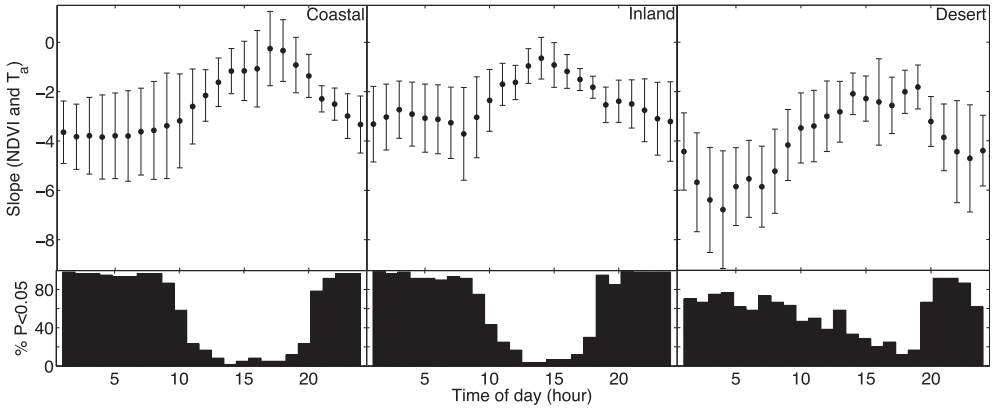


**Fig. 2.** Daily changes in slope of NDVI at 90 m radius resolution and air temperature (±SD), with frequency of P < 0.05 along the climate gradient in 2015.

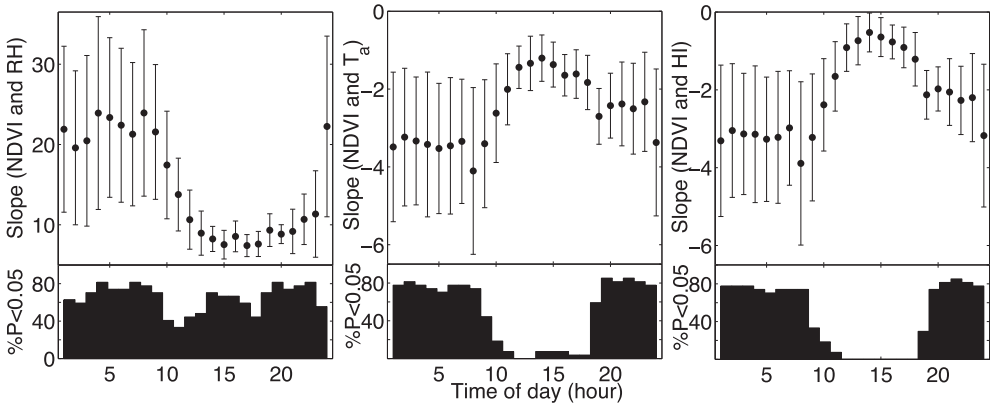


**Fig. 3.** Daily changes in slope of NDVI at 90 m radius resolution and relative humidity, air temperature, and heat index (±SD) with frequency of P < 0.05 in the inland city in 2016. Plots were in the same locations as the 2015 study (n = 20).

in the inland city, but RH of low vegetated plots decreased by 4.93% ± 4.36 (P < 0.01).

### 3.2. Vegetation and climate effects on air temperature variability

Temporal variation in $T_a$ increased with NDVI at the 90 m radius scale in the coastal, inland, and desert cities, with consistent relationships along the climate gradient (Fig. 6). These relationships have similar slopes across the climate gradient for both seasonal (Slope = 5.3, 3.0, and 4.9, respectively) and daily (Slope = 5.8, 4.2, and 6.0, respectively) scales, with differences in overall variation. For both temporal scales, there was higher overall variation in the inland city, with lower variation in the desert and coastal cities. Seasonal variation was higher than daily variation. The strength of these relationships was fairly consistent across the climate gradient at both seasonal ($R^2$ = 0.26, 0.25, and 0.21, respectively) and daily ($R^2$ = 0.29, 0.37, and 0.24, respectively) scales (P < 0.05). There were no significant correlations at the individual pixel scale (P > 0.05).

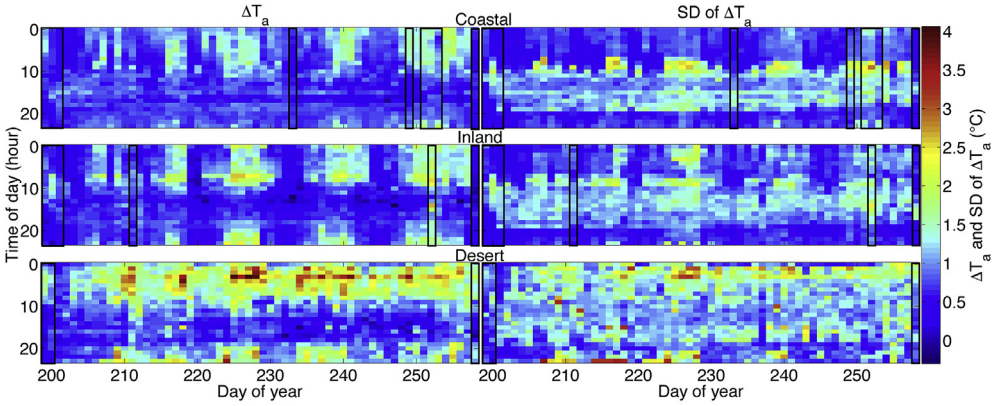


**Fig. 4.** Heat map of the local vegetation temperature effects throughout the study period, low-vegetated minus high-vegetated cover ($\Delta T_a$), with spatial standard deviation along the climate gradient. Black boxes indicate days with measurable precipitation.

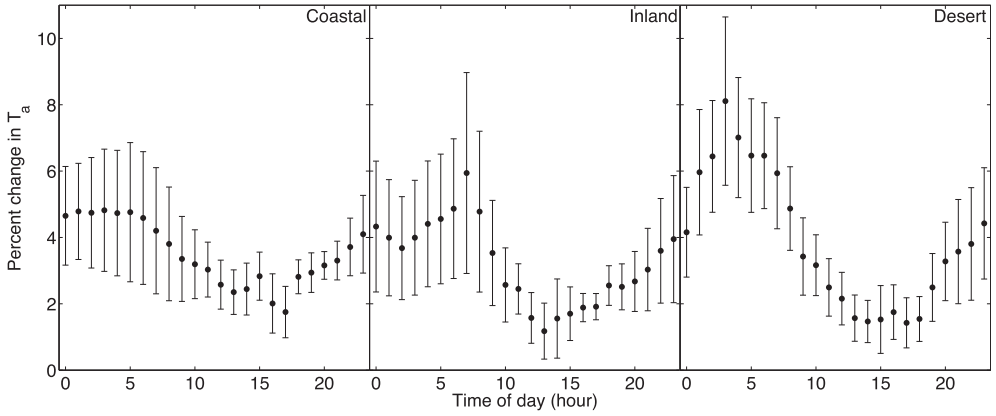


**Fig. 5.** Normalized daily temperature effects ($\Delta T_a$), or the percent change in air temperature between high- and low-vegetated plots (±SD), along the climate gradient. Low- and high-vegetated locations had little temperature difference in the day and greater difference at night. The effect increased from coastal to desert cities.

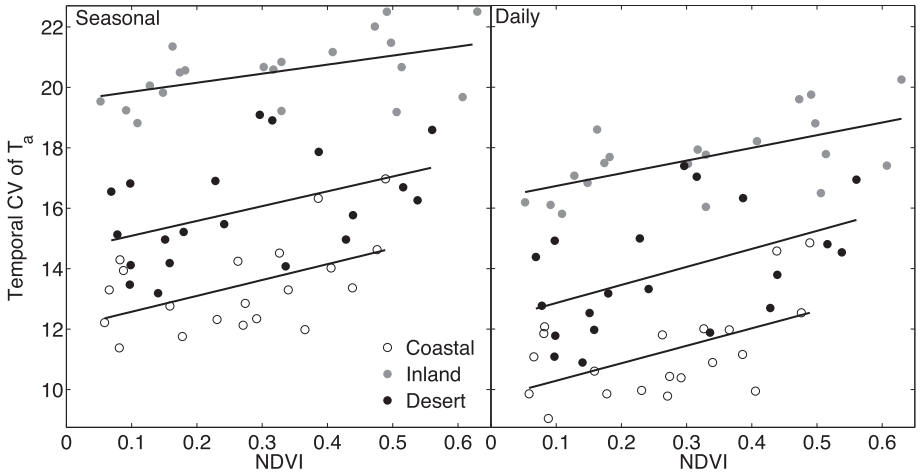


**Fig. 6.** Temporal coefficient of variation of $T_a$ was positively correlated to NDVI at 90 m radius scale in the coastal, inland, and desert cities at both seasonal ($R^2 = 0.26$,0.25, and 0.21, respectively) and daily ($R^2 = 0.29$,0.37, and 0.24, respectively) scales ($P < 0.05$). The relationships had similar slopes for both seasonal (Slope = 5.3, 3.0, and 4.9, respectively) and daily (Slope = 5.8, 4.2, and 6.0, respectively) scales across the climate gradient, with differences in overall variation. There were no significant correlations at 30 m radius scale.

Spatial variation of air temperature (CV of $T_a$) was positively correlated to mean $T_a$ for the coastal city, while negatively correlated in the inland and desert cities (Fig. 7A, Slope = 0.10, −0.07, and −0.26, respectively). Additionally, the strength of these relationships increased across the climate gradient ($R^2 = 0.07$, 0.09, and 0.40, respectively, $P < 0.05$). These relationships were not consistent throughout the day, with large daily changes (Fig. 7B). The coastal city had 12 significant positive relationships between $T_a$

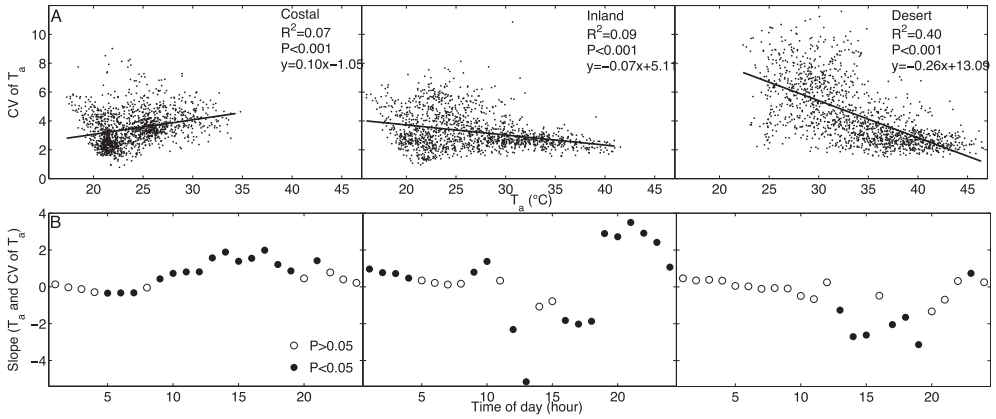


**Fig. 7. (A)** Spatial variation of air temperature (CV of $T_a$) was positively correlated to mean air temperature ($T_a$) for the coastal city, while negatively correlated in the inland and desert cities. **(B)** In the day CV of $T_a$ was positively correlated to $T_a$ for the coastal city, while negatively correlated in the inland and desert cities, with reversed patterns at night. Each data point corresponds to the slope of the linear regression between citywide mean $T_a$ and CV of $T_a$ calculated hourly (n = 60 per hour).

and CV of $T_a$ from 9:00 to 21:00, with three negative relationships between 5:00 and 7:00. The inland city had both positive and negative relationships. There were five significant negative relationships between 12:00 to 18:00, and 12 positive relationships between 16:00 to 10:00. The desert city had mostly negative relationships with six between 13:00 to 19:00, with one positive relationship at 23:00. There was a strong daily pattern in slopes ranging from −0.35 to 1.99, −5.16 to 3.50, and −3.14 to 0.74 from coastal to inland to desert cities, respectively. Daily changes in the strength of the relationship mirrored that of the slope, with r-values ranging from −0.32 to 0.60, −0.52 to 0.66, and −0.59 to 0.34 from coastal to inland to desert cities, respectively.

## 4. Discussion

We found that vegetation reduces summer $T_a$ primarily at night, or around the period when daily minimum temperatures occur. This finding supports the hypothesis that urban vegetation reduces $T_a$ through reductions in heat fluxes from impervious surfaces that had been shaded during the daytime period. Importantly, this finding is in contrast with remotely sensed LST measurements, that show vegetation cooling of urban surfaces is largest during the daytime period (Buyantuyev and Wu, 2010; Myint et al., 2013; Jenerette et al., 2016). During the daytime, urban vegetated surfaces may be directly cooled through increased evapotranspiration with large LST effects and relatively less $T_a$ cooling. Consistent with the evapotranspiration hypothesis, we observed consistent increases in RH in more vegetated areas. Evapotranspiration is not a likely mechanism explaining the effects on nighttime microclimate variation, also consistent with limited nighttime LST cooling by vegetation, because it primarily occurs during active photosynthesis. However, relationships between vegetation and RH at night were stronger than the daytime, which could be attributed to nighttime irrigation associated with urban vegetation. Nevertheless, this finding has important implications for urban microclimates in that an increasing RH may counteract the human health benefits of vegetated $T_a$ cooling at the local scale.

Across the coastal to desert climate gradient we found increasing local scale cooling effects ($\Delta T_a$) positively correlated with NDVI, confirming studies that have found increased vegetation cooling intensity in hot arid regions, contributing to a negative climate feedback effect (Imhoff et al., 2010; Tayyebi and Jenerette, 2016). As a result of greater nighttime cooling effects, higher NDVI is associated with increased $T_a$ temporal variability. This effect is reflected in seasonal scale variability, where changes in weather patterns, like heat waves, wind, and precipitation contribute to variation in addition to land cover drivers. Furthermore, supporting the $\overline{T}_a$–$T_a$ variability hypothesis we observed increased spatial variation with increasing mean temperature at the coast, however, wind may have played a larger role in inland and desert cities where there was a gradient toward decreased variation with increased mean temperature.

### 4.1. Mesoclimate and meteorological influences on microclimate variation: mean temperature, wind, and precipitation

We found large differences in the $\overline{T}_a$–$T_a$ variability relationships among cities suggesting that mesoclimate may drive vegetation microclimate cooling effects. Mean $T_a$ was positively correlated to variation of $T_a$ at the coastal city, supporting the $\overline{T}_a$–$T_a$ variability hypothesis. Counter to this hypothesis, however, inland and desert cities exhibited reduced $T_a$ variation with increased mean $T_a$ at the city scale. These seemingly contradictory findings can be better understood by examining changes in the $\overline{T}_a$–$T_a$ variability relationship throughout the day. Negative relationships in inland and desert cities are consistent with daily patterns that show stronger negative correlations during the day, with an opposite pattern in the coastal city. Spatial variation in $T_a$ was higher during warm summer nights and weakest during warm summer days for inland and desert cities, while the opposite daily trend occurred in the coastal city. Warm nights are more variable in inland and desert cities resulting in increased nighttime $T_a$ inequity between high- and low-vegetated neighborhood plots. This increased $T_a$ variation on hot nights supports the $\overline{T}_a$–$T_a$ variability hypothesis, as urban surfaces re-emit absorbed heat in the evening (Roth et al., 1989).

There are two findings that do not support the $\overline{T}_a$–$T_a$ variability hypothesis. First, $\overline{T}_a$–$T_a$ variability relationships during the day for inland and desert cities were negative. Second, although both inland and desert cities exhibited positive nighttime slopes, relationships were stronger in the inland city than in the desert city, even though the desert city is hotter. These results were partially explained by examining patterns of wind and precipitation.

While wind may have little effect on patterns of surface heat storage and fluxes, $T_a$ is influenced by air convection and mixing (Landsberg, 1981; Imhoff et al., 2010; Zhao et al., 2014). At whole city scales, temperature differences between rural and urban areas are driven by daily weather conditions and are reduced during windy days (Landsberg, 1981; Gallo et al., 1993). Using a representative meteorological station for each city, we found the inverted daily relationships of mean $T_a$ and spatial variation in inland and desert cities are partially explained by wind velocity. Wind velocity at each plot location would clarify relationships on the local dynamics of $T_a$ and wind. Here, the lack of safe mounting locations and the cost associated with installing anemometers on street-side trees at each plot ($n = 60$) precluded their deployment in our study – microclimate wind distributions remain an important research need (Vahmani and Ban-Weiss, 2016). Among cities, wind velocity is highest during the day for coastal and inland cities, and warmer days are often windier ($R^2 = 0.51$, $P < 0.001$, Supplemental Fig. 4). Air mixing with increased wind velocity on warm days can result in lower $T_a$ spatial variation. Furthermore, wind velocity is often reduced at night and there are weaker relationships between mean $T_a$ and wind velocity ($R^2 = 0.39$, $P < 0.001$, Supplemental Fig. 4). Thus at night, when wind velocity is lower, surface heat flux may more strongly drive spatial variation in $T_a$. Coastal regions, on the other hand, have different wind patterns, likely resulting in distinct diel $\overline{T}_a$–$T_a$ variability relationships. Coastal regions receive onshore wind in the daytime hours, as the land heats up faster than the neighboring ocean, which can interact with urban land cover influences on local climate (Ramamurthy and Bou-Zeid, 2017). These onshore winds reduce $T_a$, thus the warmest days are often the *least* windy days. This unique coastal wind pattern would generate the least air mixing during warm days, which in combination with existing surface heat flux, would generate greater daytime $T_a$ spatial variation.

For an initial evaluation of these predictions we compared the slope of wind velocity and variation of $T_a$ (CV of $T_a$). Correlations were found for 8 h of the day at the coastal city and 5 h of the day for the inland and desert cities (Supplemental Fig. 5). The inland city has faster winds in the day (2.37 m $s^{-1}$ from 6:00 to 20:00) than at night (0.95 m $s^{-1}$ from 20:00 to 6:00), while the desert city has similar average wind velocities both day (2.20 m $s^{-1}$) and night (2.26 m $s^{-1}$) over the entire study period. Greater daytime wind velocity in the inland city could help explain the larger daily range of correlations between wind velocity and CV of $T_a$, where higher daytime wind velocities were correlated with decreased spatial variation between 7:00 and 15:00 (Supplemental Fig. 5). Furthermore, similar average day and night wind velocities in the desert may help explain the relatively consistent statistically significant correlations between NDVI and $T_a$ in the daytime. Other weather

events, particularly precipitation, may further drive daily patterns.

Like wind, rain also reduced vegetation effects along the climate gradient likely through reduced tree shading effects, direct cooling of impervious land surfaces, and homogenization of evapotranspiration (Landsberg, 1981; Imhoff et al., 2010; Zhao et al., 2014). Some rainy days had greater reductions in vegetation effects, which are a likely result of precipitation magnitude, timing, and duration. The largest reductions in $\Delta T_a$ were on the wettest day (DOY 259). Contrary to reduced vegetation effects, there were increases in spatial variation of $T_a$ during rainy days for inland and desert cities. These increases in variation were less predictable since they were not correlated with increased vegetation effects. Examination of individual weather events on urban microclimate remains an important future research area.

### 4.2. Building on the "urban heat riskscape"

Understanding the spatiotemporal variation and drivers of vegetative cooling is important for reducing heat vulnerability (Demuzere et al., 2014; Vargo et al., 2016). We found at the local paired plot-scale (1–1.5 km) low vegetated areas have higher mean $T_a$ and lower temporal variation in $T_a$ primarily as a result of reduced nighttime vegetation cooling effects. Increases in temperatures that result from regional and global climate changes may reduce citywide $T_a$ variation in arid and semi-arid cities. Although, urban environments typically have more intricate arrangements of land covers, so factors such as changes in height-to-width ratio of the street, anthropogenic heat sources, surface albedo, tree canopy density, tree species, below tree ground cover, and tree age and vitality will likely add complexity to our findings (Taha, 1997; Shashua-Bar and Hoffman, 2000; Middle et al., 2014; Gillner et al., 2015). Furthermore, future work on the effects of buffer size when computing NDVI could refine vegetation effects on microclimate variation. Our findings in inland and desert cities are in contrast with LST studies that show warming conditions may lead to greater temperature variation between urban surfaces (Jenerette et al., 2011, 2016; Tayyebi and Jenerette, 2016). Nighttime vegetation cooling effects, important for mitigating urban warming, are driven by divergent processes across the region. While hotter nights are associated with increased spatial variation only in the inland city, exacerbating city-wide temperature inequities, there are reduced spatial effects of hotter nights in coastal and desert cities. Such regional climate considerations are important for designing geographically specific mitigation strategies.

Increasing urban vegetation is one strategy for mitigating urban warming (Larsen, 2015), but there are confounding impediments. These include economic and resources costs associated with purchasing, planting and maintaining vegetation over its entire life cycle (Jenerette et al., 2011; Pataki et al., 2011; McPherson and Kendall, 2014; Demuzere et al., 2014). Increasing vegetation offers greater nighttime cooling effects in inland and desert cities but may do little to reduce daytime $T_a$, especially on hotter days associated with higher wind velocity. Regardless, trees may decrease daytime human perceived temperatures through shading (Klemm et al., 2015; Taleghani et al., 2016). Furthermore, with increased irrigation and decreased wind velocity high-vegetated areas increase RH, subsequently increasing the HI, and potentially countering $T_a$ cooling benefits (Potchter et al., 2006). Nevertheless, we found increases in HI are minimal compared to direct cooling effects. More humid environments may be affected differently as high $T_a$ was often associated with low RH in our study system. There are a wide range strategies to reduce the effects of urban warming besides increasing urban vegetation; some of these include increasing albedo of building surfaces and spacing between buildings, and constructing a variety of different green infrastructures to increase evaporative cooling (Grimmond, 2007; Demuzere et al., 2014; Wong and Jim, 2015; Taleghani et al., 2016). Any strategy should consider trade-offs between geographic and temporally specific urban cooling benefits, and economic and resource costs.

## 5. Conclusions

We found the greatest vegetation cooling effects and $T_a$ reductions in the evening hours, with minimal effects observed during midday. This effect increased in strength from coastal to desert cities. This "U-shaped" daily $T_a$ vegetation cooling effect resulted in more daily and seasonal variation in high-vegetated areas which had a broader range of temperatures. Vegetation also increased RH and HI in the inland city, although these effects were limited. Furthermore, in the coastal city hotter days were correlated with increases in spatial variation in $T_a$ while in inland and desert cities hotter days were correlated with reductions in spatial variation, and consequently areas of temperature refuge. Nighttime spatial variation in microclimate also differed among cities. In the inland city, hotter nights were associated with increases in spatial variation in $T_a$, which likely increase inequities in urban temperatures. These patterns were partially explained by differences in wind velocity. Higher wind velocity was associated with reductions in spatial variation most in the inland areas, but this effect was not consistent across the climate gradient. Together these findings show that urban vegetation had consistent microclimate atmospheric cooling effects that primarily occur during the evening and are influenced by mesoclimate distributions and meteorological conditions.

## Acknowledgements

This study was supported by NASA through grant NNX12AQ02G, NNX15AF36G, and National Science Foundation Sustainability Research Network through grant 1444758. We thank Holly M. Andrews, Peter C. Ibsen, Cara Fertitta, Liyin L. Liang, and Isaac W. Park for field help and consultation.

## Appendix A. Supplementary data

Supplementary data related to this article can be found at http://dx.doi.org/10.1016/j.jenvman.2017.05.077.

## References

Armson, D., Rahman, M.A., Ennos, A.R., 2013. A comparison of the shading effectiveness of five street tree species in Manchester, UK. Arboric. Urban For. 39, 157–164.

Brazel, A., Selover, N., Vose, R., Heisler, G., 2000. The tale of two climates—Baltimore and Phoenix urban LTER sites. Clim. Res. 15, 123–135.

Brazel, A., Gober, P., Lee, S., Grossman-Clark, S., Zehnder, J., Hedquist, B., Comparri, E., 2007. Determinants of change in the regional urban heat island in metropolitan Phoenix (Arizona, USA) between 1990 and 2004. Clim. Res. 33, 171–182.

Buyantuyev, A., Wu, J.G., 2010. Urban heat island and landscape heterogeneity: linking spatiotemporal variations in surface temperature to land-cover and socioeconomic patterns. Landsc. Ecol. 25, 17–33.

Cao, X., Onishi, A., Chen, J., Imura, H., 2010. Quantifying the cool island intensity of urban parks using ASTER and IKONOS data. Landsc. Urban Plan. 96 (4), 224–231.

Chakraborty, S.D., Kant, Y., Mitra, D., 2015. Assessment of land surface temperature and heat fluxes over Delhi using remote sensing data. J. Environ. Manag. 148, 143–152.

Chow, W.T.L., Pope, A., Martin, C.A., Brazel, A.J., 2011. Observing and modeling the nocturnal park cool island of an arid city: horizontal and vertical impacts. Theor. Appl. Climatol. 103, 197–211.

Chow, W.T.L., Volo, T.J., Vivoni, E.R., Jenerette, G.D., Ruddell, B.L., 2014. Seasonal dynamics of energy balance in Phoenix, AZ. Int. J. Climatol. 34, 3863–3880.

Coseo, P., Larsen, L., 2014. How factors of land use/land cover, building configuration, and adjacent heat sources and sinks explain Urban Heat Islands in Chicago. Landsc. Urban Plan. 125, 117–129.
Crum, S.M., Liang, L.L., Jenerette, G.D., 2016. Landscape position influences soil respiration variability and sensitivity to physiological drivers in mixed-use lands of Southern California, USA. J. Geophys. Res. Biogeosci. 121 http://dx.doi.org/10.1002/2016JG003469.
Davis, A.Y., Jung, J., Pijanowski, B.C., Minor, E.S., 2016. Combined vegetation volume and "greenness" affect urban air temperature. Appl. Geogr. 71, 106–114.
Declet-Barreto, J., Brazel, A.J., Martin, C.A., Chow, W.T.L., Harlan, S.L., 2013. Creating the park cool island in an inner-city neighborhood: heat mitigation strategy for Phoenix, AZ. Urban Ecosyst. 16 (3), 617–635.
Demuzere, M., Orru, K., Heidrich, O., Olazabal, E., Geneletti, D., Orru, H., Bhave, A.G., Mittal, N., Feliu, E., Faehnle, M., 2014. Mitigating and adapting to climate change: multi-functional and multi-scale assessment of green urban infrastructure. J. Environ. Manag. 146, 107–115.
Feyisa, G.L., Dons, K., Meilby, H., 2014. Efficiency of parks in mitigating urban heat island effect: an example from Addis Ababa. Landsc. Urban Plan. 123, 87–95.
Gallo, K.P., McNab, A.L., Karl, T.R., Brown, J.F., Hood, J.J., Tarpley, J.D., 1993. The use of a vegetation index for assessment of the urban heat island effect. Int. J. Remote Sens. 14 (11), 2223–2230.
Gillner, S., Vogt, J., Dettman, S., Roloff, A., 2015. Role of street trees in mitigating effects of heat and drought at highly sealed urban sites. Landsc. Urban Plan. 143, 33–42.
Grimm, N.B., Grove, J.M., Pickett, S.T., Redman, C.L., 2000. Integrated approaches to long-term studies of urban ecological systems. BioScience 50 (7), 571–584.
Grimmond, S., 2007. Urbanization and global environmental change: local effects of urban warming. Geogr. J. 173 (1), 83–88.
Hall, S.J., Learned, J., Ruddell, B., Larson, K.L., Cavender-Bares, J., Bettez, N., Groffman, P.M., Grove, J.M., Heffernan, J.B., Hobbie, S.E., Morse, J.L., Neill, C., Nelson, K.C., O'Neil-Dunne, J.P.M., Ogden, L., Pataki, D.E., Pearse, W.D., Polsky, C., Chowdhury, R.R., Steele, M.K., Trammell, T.L.E., 2016. Convergence of microclimate in residential landscapes across diverse cities in the United States. Landsc. Ecol. 31 (1), 101–117.
Harlan, S.L., Yabiku, S.T., Larsen, L., Brazel, A.J., 2009. Household water consumption in an arid city: affluence, affordance, and attitudes. Soc. Nat. Resour. 22 (8), 691–709.
Imhoff, M.L., Zhang, P., Wolfe, R.E., Bounoua, L., 2010. Remote sensing of the urban heat island effect across biomes in the continental USA. Remote Sens. Environ. 114 (3), 504–513.
Jenerette, G.D., Harlan, S.L., Brazel, A., Jones, N., Larsen, L., Stefanov, W.L., 2007. Regional relationships between surface temperature, vegetation, and human settlement in a rapidly urbanizing ecosystem. Landsc. Ecol. 22 (3), 353–365.
Jenerette, G.D., Harlan, S.L., Stefanov, W.L., Martin, C.A., 2011. Ecosystem services and urban heat riskscape moderation: water, green spaces, and social inequality in Phoenix, USA. Ecol. Appl. 21 (7), 2637–2651.
Jenerette, G.D., Miller, G., Buyantuev, A., Pataki, D.E., Gillespie, T.W., Pincetl, S., 2013. Urban vegetation and income segregation in drylands: a synthesis of seven metropolitan regions in the southwestern United States. Environ. Res. Lett. 8 (4) http://dx.doi.org/10.1088./1748-9326/8/4/044001.
Jenerette, G.D., Harlan, S.L., Buyantuev, A., Stefanov, W.L., Declet-Barreto, J., Ruddell, B.L., Myint, S.W., Kaplan, S., Li, X., 2016. Micro-scale urban surface temperatures are related to land-cover features and residential heat related health impacts in Phoenix, AZ USA. Landsc. Ecol. 31, 745–760.
Klemm, W., Heusinkveld, B.G., Lenzholzer, S., van Hove, B., 2015. Street greenery and its physical and psychological impact on thermal comfort. Landsc. Urban Plan. 138, 87–98.
Landsberg, H.E., 1981. The Urban Climate. Academic Press, New York, NY, USA.
Larsen, L., 2015. Urban climate and adaptation strategies. Front. Ecol. Environ. 13, 486–492.
Lazzarini, M., Marpu, P.R., Ghedira, H., 2013. Temperature-land cover interactions: the inversion of urban heat island phenomenon in desert city areas. Remote Sens. Environ. 130, 136–152.
Liang LL, Anderson RG, Shiflett SA, Jenerette GD Urban outdoor water use and response to drought assessed through mobile energy balance and vegetation greenness measurements. Environ. Res. Lett.. (In Revisions) Final revisions requested May 18, 2017.
Lin, B.S., Lin, Y.J., 2010. Cooling effect of shade trees with different characteristics in a subtropical urban park. HortScience 45, 83–86.
McPherson, E.G., Kendall, A., 2014. A life cycle carbon dioxide inventory of the Million Trees Los Angeles program. Int. J. Life Cycle Assess. 19, 1653–1665.
Middle, A., Häb, K., Brazel, A.J., Martin, C.A., Guhathakurta, S., 2014. Impact of urban form and design on mid-afternoon microclimate in Phoenix Local Climate Zones. Landsc. Urban Plan. 122, 16–28.
Myint, S.W., Wentz, E.A., Brazel, A.J., Quattrochi, D.A., 2013. The impact of distinct anthropogenic and vegetation features on urban warming. Landsc. Ecol. 28, 959–978.
Oke, T.R., 1973. City size and the urban heat island. Atmos. Environ. 7, 769–779.
Osborne, J.W., Overbay, A., 2004. The power of outliers (and why researchers should ALWAYS check for them). Pract. Assess. Res. Eval. 9 (6). Available online: http://PAREonline.net/getvn.asp?v=9&n=6.
Pataki, D.E., Boone, C.G., Hogue, T.S., Jenerette, G.D., McFadden, J.P., Pincetl, S., 2011. Ecohydrology bearings-invited commentary socio-ecohydrology and the urban water challenge. Ecohydrology 4, 341–347.
Potchter, O., Cohen, P., Bitan, A., 2006. Climatic behavior of various urban parks during hot and humid summer in the Mediterranean city of Tel Aviv, Israel. Int. J. Climatol. 26 (12), 1695–1711.
Ramamurthy, P., Bou-Zeid, E., 2017. Heatwaves and urban heat islands: a comparative analysis of multiple cities. J. Geophys. Res. Atmos. 122, 168–178.
Roberts, D.A., Dennison, P.E., Roth, K.L., Dudley, K., Hully, G., 2015. Relationships between dominant plant species, fractional cover and land surface temperature in Mediterranean ecosystem. Remote Sens. Environ. 167, 152–167.
Roth, M., Oke, T.R., Emery, W.J., 1989. Satellite-derived urban heat islands from three coastal cities and the utilization of such data in urban climatology. Int. J. Remote Sens. 10, 1699–1720.
Rothfusz, L.P., 1990. Heat Index "equation" (Or, More than You Ever Wanted to Know about Heat Index). NWS technical attachment SR 90-23. National Weather Service. http://www.srh.noaa.gov/images/ffc/pdf/ta_htindx.PDF.
Santamouris, M., 2015. Analyzing the heat island magnitude and characteristics in one hundred Asian and Australian cities and regions. Sci. Total Environ. 512, 582–598.
Shashua-Bar, I., Hoffman, M.E., 2000. Vegetation as a climatic component in the design of an urban street: an empirical model for predicting the cooling effect of urban green areas with trees. Energy Build. 31, 221–235.
Shiflett, S.A., Liang, L.L., Crum, S.M., Feyisa, G.L., Wang, J., Jenerette, G.D., 2017. Variation in the urban vegetation, surface temperature, air temperature nexus. Sci. Total Environ. 579, 495–505.
Skelhorn, C., Lindley, S., Levermore, G., 2014. The impact of vegetation types on air and surface temperatures in a temperate city: a fine scale assessment in Manchester, UK. Landsc. Urban Plan. 121, 129–140.
Souch, C.A., Souch, C., 1993. The effect of trees on summertime below canopy urban climates: a case study Bloomington, Indiana. J. Arboric. 19, 303–312.
Steadman, R.G., 1979. The assessment of sultriness. Part I: a temperature-humidity index based on human physiology and clothing science. Am. Meteorol. Soc. 18, 861–873.
Stone, B., Vargo, J., Habeeb, D., 2012. Managing climate change in cities: will climate action plans work? Landsc. Urban Plan. 107 (3), 263–271.
Streiling, S., Matzarakis, A., 2003. Influence of single and small clusters of trees on the bioclimate of a city: a case study. J. Arboric. 29, 309–316.
Taha, H., 1997. Urban climates and heat islands: albedo, evapotranspiration, and anthropogenic heat. Energy Build. 25, 99–103.
Taleghani, M., Sailor, D., Ban-Weiss, G.A., 2016. Micrometeorological simulations to predict the impacts of heat mitigation strategies on pedestrian thermal comfort in a Los Angeles neighborhood. Environ. Res. Lett. 11 (2) http://dx.doi.org/10.1088/1748-9326/11/2/024003.
Tayyebi, A., Jenerette, G.D., 2016. Increases in the climate change adaptation effectiveness and availability of vegetation across a coastal to desert climate gradient in metropolitan Los Angeles, CA, USA. Sci. Total Environ. 548–549, 60–71.
Tucker, C.J., 1979. Red and photographic infrared linear combinations for monitoring vegetation. Remote Sens. Environ. 8, 127–150.
Turner, D.P., Cohen, W.B., Kennedy, R.E., Fassnacht, K.S., Briggs, J.M., 1999. Relationships between leaf area index and Landsat TM spectral vegetation indices across three temperate zone sites. Remote Sens. Environ. 70, 52–68.
Vahmani, P., Ban-Weiss, G.A., 2016. Climatic consequences of adopting drought-tolerant vegetation over Los Angeles as a response to California drought. Geophys. Res. Lett. 43, 8240–8249.
van Leeuwen, W.J.D., Orr, B.J., Marsh, S.E., Herrmann, S.M., 2006. Multi-sensor NDVI data continuity: uncertainties and implications for vegetation monitoring applications. Remote Sens. Environ. 100, 67–81.
Vargo, J., Stone, B., Habeeb, D., Liu, P., Russell, A., 2016. The social and spatial distribution of temperature-related health impacts from urban heat island reduction policies. Environ. Sci. Policy 66, 366–374.
Wong, G.K.L., Jim, C.Y., 2015. Identifying keystone meteorological factors of green-roof stormwater retention to inform design and planning. Landsc. Urban Plan. 143, 173–182.
Yang, F., Lau, S.S.Y., Qian, F., 2011. Urban design to lower summertime outdoor temperatures: an empirical study on high-rise housing in Shanghai. Build. Environ. 46, 769–785.
Zhao, L., Lee, X., Smith, R.B., Oleson, K., 2014. Strong contributions of local background climate to urban heat islands. Nature 511, 216–219.